Pergamon

Int. J. Heat Mass Transfer. Vol. 41, No. 10, pp. 1167–1175, 1998

Printed in Great Britain
0017-9310/98 $19.00+0.00

PII: S0017-9310(97)00223-8

Void fraction measurements in boiling cryogenic mixtures using gamma densitometer

R. BØE

Department of Refrigeration and Air Conditioning, Norwegian University of Science and Technology, N-7034 Trondheim, Norway

(*Received* 30 *December* 1996 *and in final form* 24 *July* 1997)

Abstract—The void fraction in the boiling layer of liquefied natural gas is one of the parameters used to characterize the cryogen–water mixture when formulating predictive models for rapid phase transitions (RPT). With the experimental apparatus described herein for measuring the void fraction in boiling hydrocarbon mixtures, the calibration point for single-phase liquid was not possible to obtain directly. In addition, the composition of a boiling mixture changes continuously. Two different methods are described for the estimation of the chemical composition, and thereby the liquid properties. The results showed little sensitivity to the liquid properties, regarding the void fraction value. © 1998 Elsevier Science Ltd.

INTRODUCTION

As part of the efforts to construct predictive models for the energy yield from rapid phase transitions (RPT) following spills of liquefied natural gas (LNG) onto water, laboratory-scale experiments investigating boiling of liquefied hydrocarbon mixtures on a water surface were carried out. An RPT is best explained as an "explosive evaporation", which may occur in situations where two liquids come into contact, the one having a higher temperature than the boiling point of the other.

The main results from this study was that the boil-off rate, and thereby the heat flux, for the hydrocarbon mixtures was found to be much higher than for pure liquid methane, when boiling on water. The details of this study are described in ref. [1].

Parallel measurements of the void fraction in the boiling layer of hydrocarbons were also carried out during this study. In most of the proposed models for description of RPTs in cryogen–water systems, the predicted values of pressure and propagation velocity are sensitive to the value of the void fraction. Thus the aim of these measurements was merely to quantify the void fraction in the boiling layer. As this article describes, this is a straightforward task for pure methane with constant properties, and a slightly more subtle one in the case of boiling hydrocarbon mixtures, where the composition (and thereby the liquid properties) change continuously.

In two-phase flow measurements, the geometric distribution of the two phases affects the signal conversion method. Two extreme configurations are shown by Petrick and Swanson [2], in which the phases are distributed in layers parallel or perpendicular to the beam. The parallel distribution gives the following expression for the void fraction:

$$\varepsilon = \frac{F - F_l}{F_g - F_l} \tag{1}$$

while the perpendicular distribution yields

$$\varepsilon = \frac{\ln(F/F_l)}{\ln(F_g/F_l)}. \tag{2}$$

In a real situation the configuration will lie somewhere in between these two extremes, but the authors tend to favour eqn (2). This expression is also used throughout this article.

F is the photon rate measured for an arbitrary void fraction, F_l and F_g are the calibrated values, i.e. the photon rates measured for single-phase liquid and single-phase vapour, respectively. Equation (2) arises from the exponential decay law for gamma ray attenuation:

$$F = F_0 \cdot e^{-\mu\rho z}. \tag{3}$$

F_0 is the photon rate of the original beam, ρ is the density of the medium and z is the distance travelled by the beam in the absorbing material. The mass attenuation coefficient, μ, is a parameter specific to the material of the absorber and to the energy of the photons.

The liquids involved in the present study consisted of binary mixtures of methane–ethane and methane–propane, compounds with low atomic numbers. The isotope used in the gamma densitometer was Cs-137, with main photon energy of 662 keV. For this combination, the dominating attenuation mechanism is Compton scattering [3] (p. 712), where a photon upon interaction with the particles in the absorber, results in a secondary photon of lower energy, plus an electron [4].

When using a detector not being able to distinguish between different photon energies, the void fraction

NOMENCLATURE

a	parameter in model for build-up factor
B	build-up factor
E	expected value
F	photon rate [1 m^{-2} s^{-1}]
i	detector signal
i_0, i_1	instrument constants
k_{ij}	binary interaction parameter in the SRK equation
$\tilde{M}$	molecular weight
M	mass
N	molar amount
$\dot{N}$	molar boil-off rate
SD	standard deviation
T	temperature
V^*	pure component characteristic volume [l/mole]
Var	variance
w	elemental mass fraction
x	mass fraction in liquid
$\tilde{x}$	mole fraction in liquid
$\tilde{y}$	mole fraction in vapour
z	length.

Greek symbols

ε	void fraction
μ	mass attenuation coefficient [cm^2 g^{-1}]
μ_a	energy absorption coefficient [cm^2 g^{-1}]
σ_s	attenuation coefficient due to Compton scattering [cm^2 g^{-1}]
ρ	density
τ	sampling interval
ω_{SRK}	acentric factor.

Subscripts

0	incident beam
1	component number 1 (methane)
2	component number 2 (ethane or propane)
A, B	fluid number
a	air
C	carbon
c	critical
g	gas/vapour
H	hydrogen
i, j, k	component/element number
l	liquid
meas	measured
sat	saturated
r	reduced
w	water.

derived from eqn (2) tends to be overpredicted, because scattered photons are also detected. Fuchs and Linga [5] propose to compensate for the bias introduced by the impact from scattered photons by using the build-up factor. The build-up factor, B, is defined as the ratio of the detected photon rate to the theoretical photon rate. With eqn (3) denoting the theoretical photon rate, the measured photon rate is related to the theoretical by

$$F_{meas} = B \cdot F_0 \cdot e^{-\mu\rho z}. \tag{4}$$

Evans [3] (pp. 728–734) refers to measurements of gamma radiation from different point sources surrounded by an infinite water medium. From these results it is stated that the build-up factor to a first approximation increases linearly with the number of mean free paths traversed by the beam. The mean free path, $1/\mu\rho$, can be interpreted as the average distance a primary photon travels in a homogeneous absorber before interacting. The build-up factor may then be expressed as

$$B = 1 + a \cdot \mu\rho z. \tag{5}$$

The dimensionless parameter a is evaluated by means of energy conservation to equal the ratio of the attenuation coefficient due to Compton scattering, σ_s, which is a part of the mass attenuation coefficient, to the total absorption coefficient, μ_a, which is a measure of the energy absorbed by the medium [3] (p. 740):

$$a = \frac{\sigma_s}{\mu_a}. \tag{6}$$

According to Fuchs and Linga [5], a can be regarded as a constant for all relevant fluids, its numerical value being determined solely by the geometric configuration of the gamma densitometer setup. Thus for an arbitrary pair of fluids, A and B:

$$\frac{B_A}{B_B} = \frac{1 + a \cdot \mu_A \rho_A z}{1 + a \cdot \mu_B \rho_B z}. \tag{7}$$

Thus a may be expressed explicitly:

$$a = \frac{1 - B_A/B_B}{(B_A/B_B \cdot \mu_B \rho_B - \mu_A \rho_A) z}. \tag{8}$$

The following conversion equations are specific to the built-in electronics of the gamma detector. The output signal produced by the detector, i, is a linear function of the detected photon rate, and may thus be expressed as

$$i = i_0 + i_1 \cdot F_{meas}. \tag{9}$$

The two constants, i_0 and i_1 depend on the instrument settings, and are determined by two-point calibration.

In the current study the two points used for calibration were water and air, giving pairs of output signals (in V) and photon rates (in kHz). Thus i_0 and i_l are determined as

$$i_l = \frac{i_a - i_w}{F_a - F_w} \tag{10}$$

$$i_0 = i_a - i_l \cdot F_a. \tag{11}$$

Writing F_{meas} in eqn (9) as BF and substituting for F in eqn (2):

$$\varepsilon(i) = \frac{\ln\left(\frac{B_l}{B} \cdot \frac{i - i_0}{i_l - i_0}\right)}{\ln\left(\frac{B_l}{B_g} \cdot \frac{i_g - i_0}{i_l - i_0}\right)}. \tag{12}$$

Equation (5) formulated for a two-phase medium with the phases distributed perpendicular to the beam then becomes

$$B = 1 + a \cdot [\mu_g \rho_g \varepsilon + \mu_l \rho_l (1 - \varepsilon)]. \tag{13}$$

Combining eqn (5) for the single phases with eqn (13), the following expression is obtained, which together with eqn (12) determines ε:

$$\frac{B}{B_l} = 1 - \varepsilon + \varepsilon \cdot \frac{B_g}{B_l}. \tag{14}$$

B_l/B_g, i_l and i_g would normally be determined by two-point calibration for single-phase liquid and single-phase gas, but it is also possible to determine B_l/B_g theoretically from eqn (7). This may be convenient in the case of, for example, high pressure systems [5], as the calibration may be carried out with water and air instead of the real fluids. The only requirement is that ρ and μ are known for all the fluids. For the current measurements in boiling cryogenic liquids, this approach to the calibration becomes a necessity.

EXPERIMENTAL

Figure 1 shows the experimental setup schematically. Samples containing approximately 600 cm^3 of liquefied hydrocarbon mixture were poured from a dewar, via the spreading device, onto the water surface where it immediately started to boil.

The liquid samples consisted of pure methane and binary mixtures of methane–ethane and methane–propane. The mixtures were prepared by weighing the pure components into an evacuated container in the gas phase, and then condensing it to liquid with a Philips cryogenerator.

The water (approximately 3 l) was contained in a cylindrical cell with inner diameter 16 cm, giving an area for boiling heat transfer of approximately 200 cm^2. The inner wall of the boiling cell was made of 25 μm mylar film to minimize the thermal bridge between the water and the cryogenic liquid, and thus minimize the edge effects.

The total mass of the boiling liquid was monitored by an electronic balance, and fast-response thermocouples (wire diameter 70 μm) monitored the temperature at three locations: in the boiling liquid, in the vapour and in the water close to the surface. The same technique has been used by, amongst others, Valencia-Chávez and Reid [6] in similar boiling experiments, who used wires with diameter 25 μm in the vapour, and diameters ranging between 75 and 150 μm in the liquid.

For static measurements with the current thermocouple probes, the standard deviation was ± 0.7 K at -196°C (measurements made in liquid nitrogen). The origin of this relatively high standard deviation is believed to be the electric fields from surrounding equipment inducing noise in the thermocouple wires, see Appendix A.

A spreading device, which was supported independently of the cell, served the purpose of damping the inertial impact from the falling cryogen on the balance by directing the liquid horizontally towards the wall.

All the measurements, including the signal from the gamma detector, were sampled to a computer file at intervals of 0.096 s.

The gamma densitometer was of the type BTG DT-9110, and designed for measurements in process pipelines up to 400 mm outer diameter. A Cs-137 source (photon energy 662 keV) of activity 1 Ci was used. To retrieve information from a horizontal layer, a collimator consisting of two massive lead bars was placed in front of the detector. The horizontal gap between the bars was 4 mm. Normally the centre of the beam traversed the boiling layer at a height of 13 mm above the water surface.

The detector produced an electric signal, proportional to the detected photon rate [see eqn (9)].

Immediately before an experiment was run, the initial composition of the liquid was measured by retrieving a small amount through a submerged cannula, which evaporated into an evacuated sample cylinder. This vapour was later analysed in a gas chromatograph.

Calibration

As mentioned in the Introduction, water and air can be used for calibration when all the fluid properties are known. With the assumption that the parameter a in the model for the build-up factor [eqn (5)] is constant for a given geometry, its numerical value may be calculated from the calibration points of water and air.

Since all the current experiments took place at atmospheric pressure, both the vapour and air density could be approximated to zero in the calculations. i_g in eqn (12) was set equal to the signal measured in air, i_a, and i_l was calculated from i_w using the theoretical value of B_l/B_w, calculated from eqn (7):

$$i_l = \frac{B_l}{B_w} \cdot \frac{e^{-\mu_l \rho_l z_0}}{e^{-\mu_w \rho_w z_0}} \cdot (i_w - i_0) + i_0. \tag{15}$$

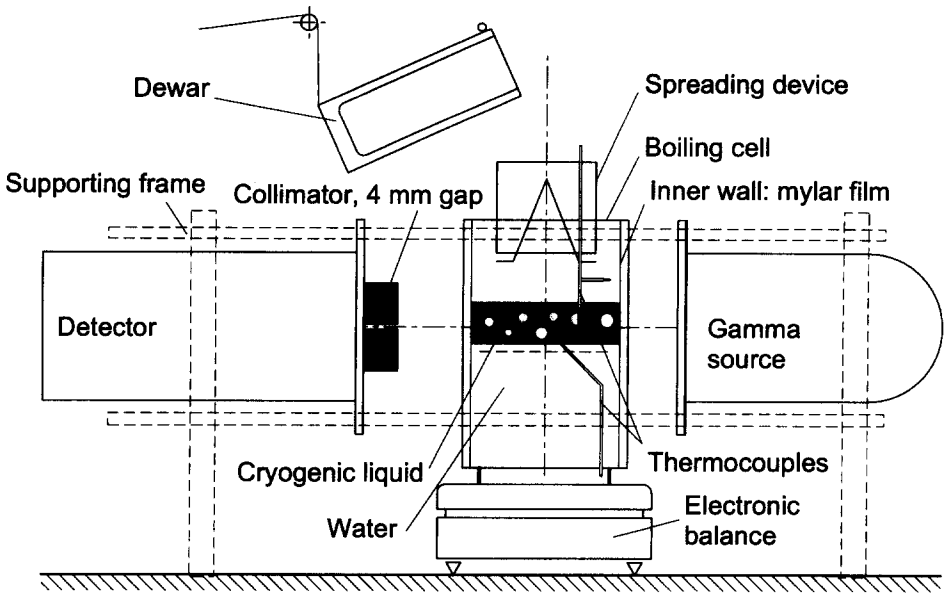

Fig. 1. Schematic view of the experimental rig.

For pure methane, ρ_l and μ_l are constant, and thus i_l was determined once and for all in the calibration procedure.

Due to the higher equilibrium concentration of methane in the vapour emanating from the boiling mixtures, the liquid remaining in the cell would gradually become deprived of methane. Both the composition and boiling point temperature would change during an experimental run, and so would μ_l and ρ_l. Hence i_l is needed to be updated for each point in the time series, and so are the estimates of the liquid properties for the mixture.

Liquid properties

For a given photon energy the mass attenuation coefficient is only dependent upon the elemental composition of the fluid, and not upon either density or phase [4]:

$$\mu = \sum_i w_i \cdot \mu_i. \tag{16}$$

w_i is the mass fraction of element i in the substance, and eqn (16) is valid both for pure chemical compounds and for mixtures. The mass attenuation coefficients for single elements are tabulated values.

Although the gas chromatography analysis showed traces of the atmospheric gases O_2 and N_2, the mixtures were assumed binary when estimating the liquid properties, thus the only elements in question were hydrogen and carbon. Assuming that the molar compositions $\tilde{x}_i$ were known, the corresponding mass fractions could be readily obtained from the molecular weight of each pure component:

$$x_i = \tilde{x}_i \cdot \frac{\tilde{M}_i}{\Sigma \tilde{x}_j \tilde{M}_j}. \tag{17}$$

The elemental mass fractions of the pure compounds were then obtained from the chemical formula and the atomic masses of the elements, given in the periodic table. For binary hydrocarbon mixtures, the elemental mass fractions of hydrogen and carbon are

$$w_H = x_1 \cdot w_{H,1} + x_2 \cdot w_{H,2} \tag{18}$$

$$w_C = x_1 \cdot w_{C,1} + x_2 \cdot w_{C,2}. \tag{19}$$

To correlate the density of saturated liquid mixtures, the Hankinson–Brobst–Thomson (HBT) correlation is recommended [7], see also Appendix B. Apart from the pure component parameters, the molar composition and the saturation temperature of the mixture are required as input to the correlation. Thus it was necessary to estimate the chemical composition of the liquid at any point during an experiment.

Liquid composition

Two approaches were made to carry out the estimation of the chemical composition of the liquid. The first method took advantage of the one-to-one relationship between composition and the boiling point temperature, which exists both for the methane–ethane and the methane–propane system. This method is illustrated in Fig. 2 for the methane–ethane system. For each point in the time series, the temperature measured in the boiling liquid was used as input to a routine that interpolated $\tilde{x}$ as a function of T_l. The interpolating functions were constructed by determining the boiling point temperature for nine intermediate $\tilde{x}$-values in each binary system by bubble-point flash calculations using the Soave–Redlich–Kwong (SRK) equation of state.

For all hydrocarbon pairs, and pairs involving

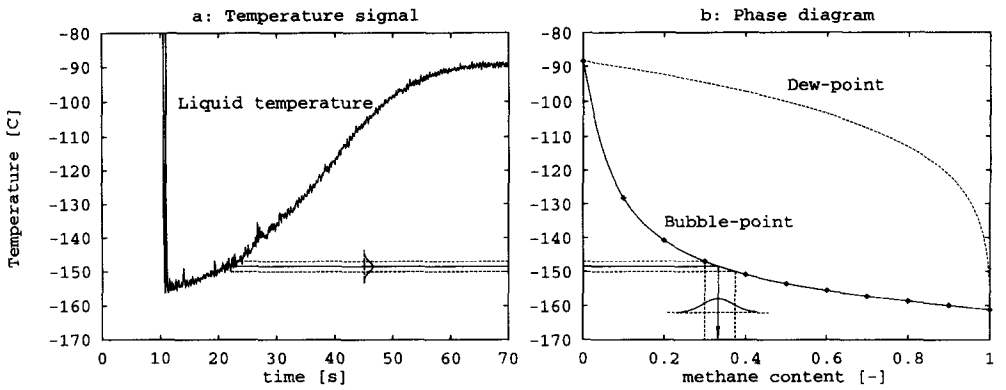

Fig. 2. Methane content estimated from liquid saturation temperature.

Table 1. Binary interaction parameters for nitrogen used in the SRK equation of state

Hydrocarbon	$k_{i,j}$
Methane	0.028
Ethane	0.041
Propane	0.076

oxygen, the binary interaction parameters were set to zero in the flash calculations. For nitrogen, the binary interaction parameters were adopted from Reid *et al.* [7], and are given in Table 1.

When interpolating these 11 points (nine + one for each pure component) by natural cubic splines, the bubble point curves were adequately described.

This method assumes that the liquid and vapour always are in phase equilibrium, i.e. that the liquid is at its boiling point and that no superheat is present in the vapour. Valencia-Chávez and Reid [6] report similar boiling experiments, in which vapour composition, and vapour and liquid temperatures were measured and compared to theoretical values obtained from the SRK equation of state. There was found to be good agreement between theory and measurement in this case.

The other method used the balance signal and the initial liquid composition retrieved from the gas chromatography analysis of the test samples taken before each run. Assuming equilibrium at all times, an ageing calculation could be used to keep track of the composition in the remaining liquid, as long as the initial mass and initial composition were known. For each increment to a lower value of M detected in the balance signal, the ageing calculation was carried out between the two successive values of M, see Fig. 3. From current estimates of the composition vector, the mole weight of the mixture was calculated and M converted to the molar value N. The change in the total molar amount of each component is related to the molar boil-off rate, $\dot{N}$, by

$$\frac{dN_i}{dt} = \frac{d(N \cdot \tilde{x}_i)}{dt} = -\dot{N}\tilde{y}_i. \tag{20}$$

Noting that $\dot{N} = -(dN/dt)$, the ageing equation is obtained:

$$\frac{dN}{N} = \frac{d\tilde{x}_i}{\tilde{y}_i - \tilde{x}_i}. \tag{21}$$

$\tilde{y}_i$ is the vapour composition in equilibrium with $\tilde{x}_i$. Having obtained an estimate for the chemical composition, the liquid density was calculated from eqns (B1)–(B8), in Appendix B.

The attenuation coefficient was calculated from eqn (16), after converting the estimated molar composition into elemental mass fractions through eqns (17)–(19).

The correlations for liquid density and mass attenuation coefficient for the methane–ethane system are depicted in Fig. 4.

Inaccuracies

The strong collimation of the gamma beam combined with the short sampling interval caused significant statistic spread in the gamma signal. Assuming a Poisson distribution for the number of photons emitted within a given time interval, τ, which has the property that $\mathrm{Var}(N) = \mathrm{E}(N) = F \cdot \tau$, the standard deviation of the signal could be predicted from the average observed photon rate and the sampling interval, τ:

$$\mathrm{SD}(i) = |i_1| \sqrt{\frac{F}{\tau}}. \tag{22}$$

An expression for the derivative of ε with respect to i is obtained from eqn (12), and so the standard deviation in void fraction due to statistical fluctuations in the radiative emission could be estimated theoretically:

$$\mathrm{SD}(\varepsilon) = \left| \frac{i_1}{\left[(i - i_0) \cdot \ln\left(\frac{B_l}{B_g} \cdot \frac{i_g - i_0}{i_l - i_0} \right) \right]} \right| \cdot \sqrt{\frac{F}{\tau}}. \tag{23}$$

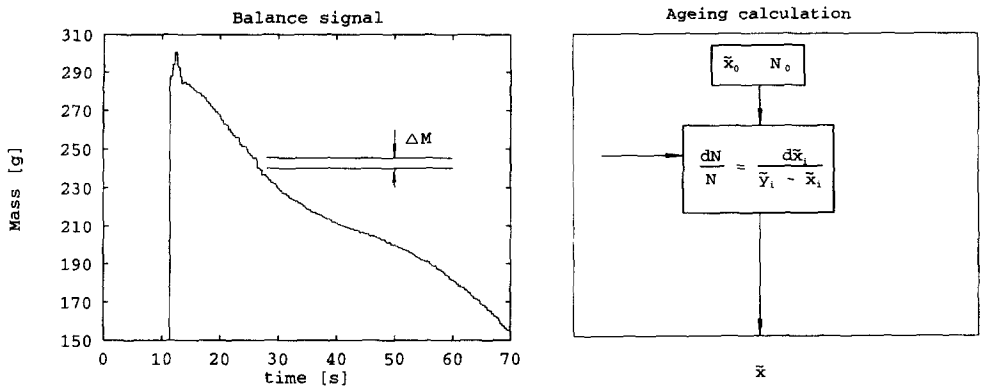

Fig. 3. Methane content estimated from ageing calculation.

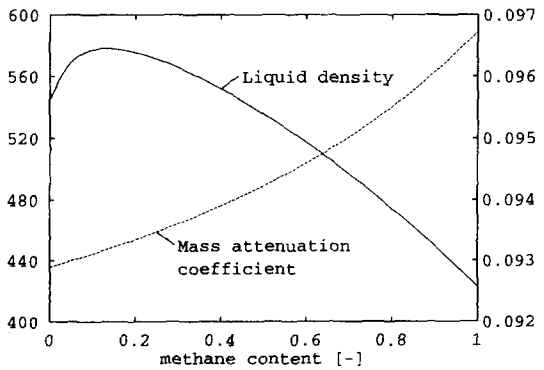

Fig. 4. Liquid density in kg m^{-3} (left-hand scale) and mass attenuation coefficient in cm^2 g^{-1} (right-hand scale) for the methane–ethane system.

When using the first estimation method (Fig. 2), the random error in the temperature signal will propagate to both ρ_l and μ_l. At high methane content it is also apparent that this error will be severely amplified because of the slope of the bubble-point curve.

During the spilling procedure, some methane will flash before the cryogenic liquid settles on the water surface. Thus there may be inconsistency between the initial composition and the initial mass when using method 2. This may cause some systematic error.

RESULTS

Figure 5 shows the void fraction vs time for a pure methane run and for a methane–ethane mixture with initial methane content $\bar{x}_0 = 0.457$. The water temperature was about 40°C in both cases. The abrupt fall in void fraction from about one early in the runs marks the time when the liquid is poured into the cell. The increase in ε between 40 and 70 s in Fig. 5(a), occurs when the liquid head decreases. Measurements taken at different heights above the water surface in some of the pure methane runs, showed that the void fraction gradually increased in the upper part of the liquid layer.

Method 1, based on the measured liquid temperature and the binary bubble-point curve, was used to estimate the liquid properties for the mixture in Fig. 5(b). The properties are constants for pure methane.

Figure 6 shows the values of $\bar{x}$ calculated with the two methods, for two different runs. The curves in Fig. 6(a) are from the same run as is shown in Figs 2, 3 and 5(b) ($\bar{x}_0 = 0.457$).

Figure 6(b) shows the estimated $\bar{x}$ for a methane–ethane run where the measured initial composition was 0.835. The estimate from method 1 is obviously erroneous in this case, but this graph is included to illustrate that the resulting void fraction comes out with very little difference between the two methods, in spite of large disagreement in $\bar{x}$, see Fig. 7.

Table 2 shows the calibration points for water, air and single-phase liquid nitrogen (LIN), measured in a Dewar flask with inner diameter 10.6 cm. In this container, a cryogenic liquid could be kept without the presence of bubbles, which was impossible in the boiling cell. The value for i_l estimated from eqn (15) was 3.211 V.

Table 3 shows the standard deviations in signal value (raw data) and void fraction measured in single-phase water and single-phase air. The corresponding values calculated from eqns (22) and (23) are also shown.

DISCUSSION

The peak in Fig. 5(b), between 15 and 30 s, is believed to result from foaming of the liquid. Visual observations made on some occasions, revealed that these periods of high void fraction coincided with the presence of foam in the boiling layer. For the example shown here, the foaming apparently ceases at $t \approx 30$ s. The methane content in the liquid is approximately 20% at this time, according to Figs 2 and 6(a).

For the majority of the mixture runs, which took place with mixtures above 80% initial methane content, the void fraction signals came out with much the same appearance as in Fig. 7. In these cases the gamma beam goes above the liquid layer when the

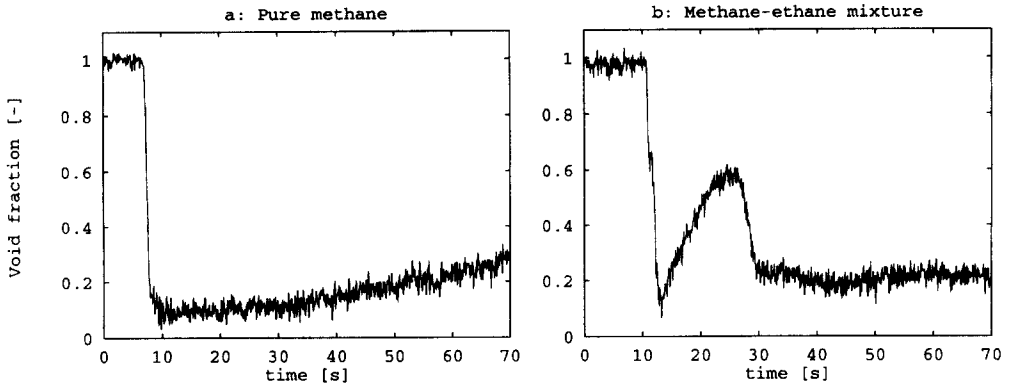

Fig. 5. Void fraction vs time for pure methane and methane–ethane mixture with initial methane content 0.457.

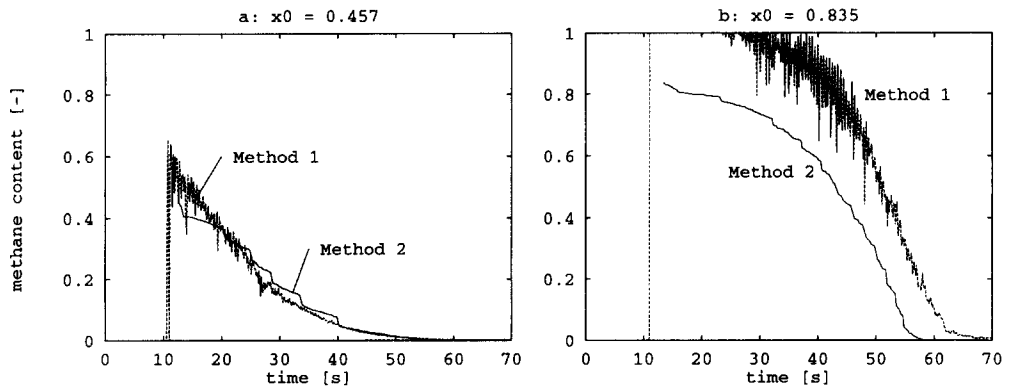

Fig. 6. Comparison between the two estimation methods for the methane content, for two different runs.

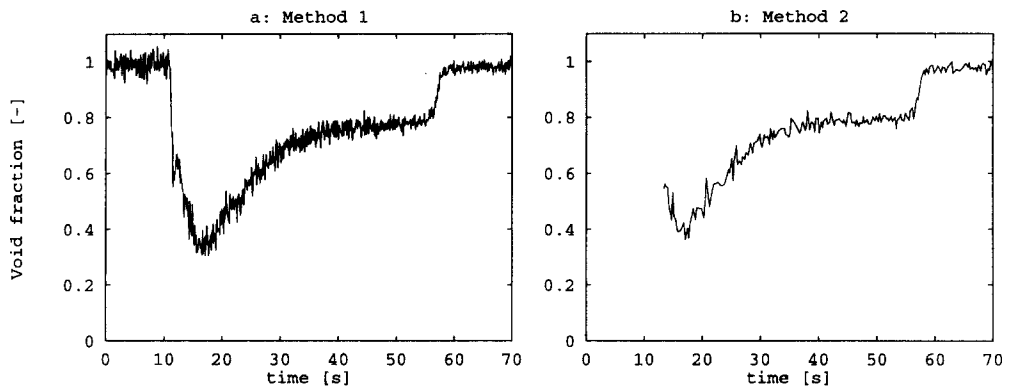

Fig. 7. Void fraction vs time for methane–ethane mixture with initial methane content 0.835, for the two different estimation methods.

Table 2. Calibration signals measured in a Dewar

Fluid	i [V], measured
Water (i_w)	3.736
LIN (i_l)	3.218
Air (i_a)	1.075

foaming ceases. Foaming did not occur in the pure methane runs.

When looking at the void fraction curves in Fig. 7, where the liquid composition is estimated by the two different methods, they appear to be almost identical, except for the smaller number of points in the time series and the absence of the part prior to the liquid spill in (b). The significant disagreement between the two methods in estimating $\tilde{x}$ in this case, shown in Fig.

Table 3. Standard deviation in signal and void fraction compared with theoretical values

Fluid	$SD(i)_{meas.}$	$SD(i)_{calc.}$ [eqn (22)]	$SD(\varepsilon)_{meas.}$	$SD(\varepsilon)_{calc.}$ [eqn (23)]
Air	$2.80 \cdot 10^{-2}$	$2.66 \cdot 10^{-2}$	$9.61 \cdot 10^{-3}$	$9.34 \cdot 10^{-3}$
Water	$1.62 \cdot 10^{-2}$	$1.38 \cdot 10^{-2}$	$2.09 \cdot 10^{-2}$	$1.82 \cdot 10^{-2}$

6(b), was probably due to an error in the temperature measurement. A reading of a few K too low in the liquid temperature causes a too high value for the composition estimated from the spline functions. This systematic error shows up in the form of an over-predicted attenuation coefficient and an under-predicted density (see Fig. 4). As these two always appear as the product of each other in the calculations, this tends to cancel the effect of the wrong estimate in $\tilde{x}$. This, together with the result in Fig. 7, suggests that the void fraction calculation is relatively insensitive to errors in the liquid properties.

The difference between the measured value of i and the value calculated for LIN in Table 2 is about 0.3% of the range (0.007 V compared to 2.661 V). This good agreement is taken as an indication that this calibration method works well in general.

Agreement between measured and theoretical values for the standard deviation in both i and ε is apparent in Table 3. For the signal value, which is proportional to the photon rate [eqn (9)], it can be shown that the standard deviation is proportional to the square root of the photon rate. This is a characteristic property of the Poisson distribution. The random error in i is thus largest at the higher range of the void fraction.

The standard deviation in the void fraction is, on the contrary, smaller at the higher range of void fraction, and this is due to the unlinear conversion characteristics.

The majority of the spread in ε is believed to arise from the statistical spread in the signal value i.

CONCLUSION

- The numerical value of the void fraction measured in a layer of pure liquid methane boiling on a water surface is in the range 0.1–0.2, as long as the liquid layer covers the gamma beam. For binary mixtures the void fraction attains high values, typically 0.5–0.8, due to the presence of foam.
- Estimation of the liquid composition in binary hydrocarbon mixtures using the measured boiling point temperature, resulted in a large spread in the estimates for high methane content. This occurred due to the propagation of the error from the temperature signal.
- In one case, where the liquid composition estimated from the balance signal and the ageing calculation gave a result very different from the one estimated from the bubble-point curve, the resulting void fraction values differed only slightly when comparing the two methods. The calculation procedure for void fraction is thus quite insensitive to errors and variations in the liquid properties.
- Calibration of the gamma densitometer for water–air with the use of a linear model for the build-up factor, gave a correct estimate of the calibration signal for pure liquid nitrogen.
- Most of the spread in void fraction is due to the statistical spread in the gamma emission, which propagates through the calculations to the signal value.

Acknowledgements—The research described herein was financed by Statoil R & D, Trondheim, and The Norwegian University of Science and Technology, Trondheim, Norway.

REFERENCES

1. Bøe, R., Pool boiling of hydrocarbon mixtures on water. Dr.ing. Thesis, Norwegian University of Science and Technology, Trondheim, 1996.
2. Petrick, M. and Swanson, B. S., Radiation attenuation method of measuring density of a two-phase fluid. *The Review of Scientific Instruments*, 1958, **29**(12), 1079–1085.
3. Evans, R. D., *The Atomic Nucleus*. McGraw-Hill, New York, 1955.
4. Debertin, K. and Helmer, R. G., *Gamma- and X-ray Spectrometry with Semi-conductor Detectors*. North-Holland, Amsterdam, 1988, pp. 29–39.
5. Fuchs, P. and Linga, H., Impact from scattered photons on void fraction measurements with gamma densitometers. Paper G4, European Two-Phase Flow Group Meeting, Rome, 1991.
6. Valencia-Chávez, J. A. and Reid, R. C., The effect of composition on the boiling rates of liquefied natural gas for confined spills on water. *International Journal of Heat and Mass Transfer*, 1979, **22**, 831–838.
7. Reid, R. C., Prausnitz, J. M. and Poling, B. E., *The Properties of Gases & Liquids*, 4th edn. McGraw-Hill, New York, 1987.

APPENDIX A

To measure the static accuracy of the temperature measurements, signal recordings in ice-water and liquid nitrogen were made for each of the two thermocouple probes located in the cryogen. The boiling point for nitrogen and the freezing point for water correspond to the two outermost ends of the calibrated range of the thermocouples. The sampling interval $\tau = 0.096$ s was used. From these time series, the mean value and standard deviation in the signal was

Table A1. Measured temperature mean values and standard deviation

Condition	Probe	$\bar{T}$ [°C]	SD [K]
Ice/water	1	−0.2126	0.3762
	2	−0.3325	0.2791
LIN	1	−196.2	0.6993
	2	−196.7	0.4651

calculated after converting the raw data into temperatures. The numerical results are shown in Table A1.

The power spectrum for one of the runs is shown in Fig. A1. It shows marked peaks at 2 and 2.5 Hz. It is believed that the peaks in the spectrum are reflections of the alternating current frequency at 50 Hz, induced in the thermocouple wires by the noise from electric equipment. The power spectrum of a computer generated signal of exactly 50 Hz is also shown in Fig. A1, and the peak from this coincides with the largest peak for the measured signal.

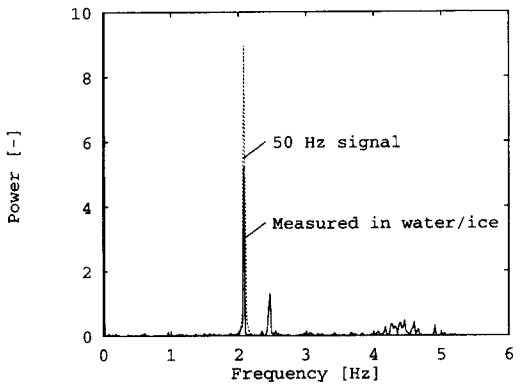

Fig. A1. Power spectrum for static temperature measurement in water/ice compared with the power spectrum for a sine function at 50 Hz.

APPENDIX B

The Hankinson–Brobst–Thomson correlation for the density of saturated liquid mixtures: for $0.25 < T_r < 0.95$, the density in mole l^{-1} is given by

$$\frac{1}{\rho} = V^* V_R^0 (1 - \omega_{SRK} V_R^\delta) \tag{B1}$$

$$V_R^0 = 1 + a(1-T_r)^{1/3} + b(1-T_r)^{2/3} + c(1-T_r) + d(1-T_r)^{4/3} \tag{B2}$$

$$V_R^\delta = (e + fT_r + gT_r^2 + hT_r^3)/(T_r - 1.00001) \tag{B3}$$

$$T_r = \frac{T_{sat}}{T_c}. \tag{B4}$$

Mixing rules (pure component parameters are given in Table B1):

$$T_c = \frac{\Sigma_j \Sigma_k \tilde{x}_j \tilde{x}_k V_{jk}^* T_{cjk}}{V^*} \tag{B5}$$

$$V^* = 1/4 \left[\sum_j V_j^* + 3 \left(\sum_j \tilde{x}_j V_j^{*2/3} \right) \left(\sum_j \tilde{x}_j V_j^{*1/3} \right) \right] \tag{B6}$$

$$V_{jk}^* T_{cjk} = (V_j^* T_{cj} V_j^* T_{ck})^{1/2} \tag{B7}$$

$$\omega_{SRK} = \sum_j \tilde{x}_j \omega_{SRK_j}. \tag{B8}$$

Table B1. Parameters in the HBT-correlation

Coefficients in the polynomials			
$a = -1.528160$		$e = -0.2961230$	
$b = 1.439070$		$f = 0.3869140$	
$c = -0.814460$		$g = -0.0427258$	
$d = 0.190454$		$h = -0.0480645$	
Components	CH_4	C_2H_6	C_3H_8
T_{sat} [K]	111.6	184.6	231.1
T_c [K]	190.58	305.42	369.82
V^* [l mole^{-1}]	0.0994	0.1458	0.2001
ω_{SRK} [—]	0.0074	0.0983	0.1532